Emergent states in dense systems of active rods: from swarming to turbulence

2012 J. Phys.: Condens. Matter 24 464130

(http://iopscience.iop.org/0953-8984/24/46/464130)

IOP Publishing Journal of Physics: Condensed Matter
J. Phys.: Condens. Matter **24** (2012) 464130 (10pp) doi:10.1088/0953-8984/24/46/464130

Emergent states in dense systems of active rods: from swarming to turbulence

H H Wensink[1,2] **and H Löwen**[1]

[1] Institut für Theoretische Physik II: Weiche Materie, Heinrich-Heine-Universität-Düsseldorf, Universitätsstraße 1, D-40225 Düsseldorf, Germany
[2] Laboratoire de Physique des Solides, Université Paris-Sud & CNRS, Bâtiment 510, 91405 Orsay Cedex, France

E-mail: hlowen@thphy.uni-duesseldorf.de

Received 14 March 2012, in final form 25 April 2012
Published 31 October 2012
Online at stacks.iop.org/JPhysCM/24/464130

Abstract
Dense suspensions of self-propelled rod-like particles exhibit a fascinating variety of non-equilibrium phenomena. By means of computer simulations of a minimal model for rigid self-propelled colloidal rods with variable shape we explore the generic diagram of emerging states over a large range of rod densities and aspect ratios. The dynamics is studied using a simple numerical scheme for the overdamped noiseless frictional dynamics of a many-body system in which steric forces are dominant over hydrodynamic ones. The different emergent states are identified by various characteristic correlation functions and suitable order parameter fields. At low density and aspect ratio, a disordered phase with no coherent motion precedes a highly cooperative swarming state with giant number fluctuations at large aspect ratio. Conversely, at high densities weakly anisometric particles show a distinct jamming transition whereas slender particles form dynamic laning patterns. In between there is a large window corresponding to strongly vortical, turbulent flow. The different dynamical states should be verifiable in systems of swimming bacteria and artificial rod-like micro-swimmers.

(Some figures may appear in colour only in the online journal)

1. Introduction

Collections of swimming microorganisms and self-propelled particles are able to form remarkable macroscopic patterns [1–4] including swarms [5, 6] and complex vortices [7–11]. The tendency for neighbouring particles to align is strongly determined by their mutual interactions which provide the key to understanding the emergent behaviours at high particle density. In this regime, the interplay between microscopic self-motility and anisotropic volume-exclusion interactions leads to complex spatio-temporal behaviour [12, 13] that can be directly visualized in two spatial dimensions, i.e. for particles moving in planar confinement.

Quasi-two-dimensional systems of self-propelled particles can be realized in a number of ways. Autonomously navigating bacteria and other microbes can be confined to free-standing thin films [9], between solid surfaces [14] or a liquid-gas interface [8, 15]. On larger length scales, active systems can be realized by polar granulates on a vibrating surface [16–18] or pedestrians moving in complex environments [19]. Last not least, colloidal dispersions constitute ideal model systems not only for investigating passive matter [20, 21] but also for active matter composed of self-motile colloidal particles. Over the past decade, a number of distinctly different realizations of active colloidal particles have been proposed. These include Janus particles driven by catalytic processes [22, 23] or thermophoretic [24] gradients, particles propelled by artificial flagella [25] and surface waves [26, 27] driven in an external magnetic field. Rather than being spherical, most of these particles have an anisotropic rod-like shape and the intrinsic alignment of colliding particles is found to play a crucial role in determining the spatio-temporal behaviour of active particles [28–30]. Confining systems to quasi-planar geometries allows for a direct visualization of the particles by means of real-space microscopy and provides fascinating opportunities to study the single-particle and collective behaviour of micro-swimmers.

In this paper we use computer simulation to study a simple model for suspensions of rigid, self-propelled rods (SPRs) that interact via a Yukawa-segment potential [31, 32]. The potential allows for a realistic description of the strong mutual short-range repulsion that prevents particles from overlapping. Self-motility is imposed by introducing a constant propulsion force along the main orientation axis of each rod. Consequently, when two neighbouring active rods collide they align, and the aligning force plays an essential role in the formation of flocks of coherently moving particles [30, 33]. In our study we focus on the collective behaviour of dense suspensions of strongly interacting particles and characterize the emergent states by analysing different correlation functions as dynamical diagnostics. In order to retain a generic framework we consider the overdamped frictional dynamics of a many-body system where the equations of motion arise from a simple force balance between the Stokesian frictional force, the collision force and the active force on each rod. Likewise, the rod orientations propagate via a torque balance involving the frictional and interaction torque acting on each particle. Other forces due to many-body hydrodynamic interactions or thermal fluctuations exerted by the embedding solvent, for example, are neglected. This allows us to simplify the microscopic equations of motion in such a way that the rod aspect ratio and density constitute the main variational parameters of the model. The microscopic self-propulsion force can be appropriately scaled out and subsumed into an (effective) Yukawa amplitude which only has a weak impact on the emergent behaviour.

Despite its simplicity, the model is capable of predicting a wealth of different steady states that hitherto could not be realized within a single framework. Amongst the various states we identify an incoherent, disordered dynamical phase at small particle aspect ratio and a cooperative swarming state with giant number density fluctuations at larger rod anisometry as found in a number of particle-resolved models [28, 32–35]. At high densities and small aspect ratios, we find a jammed phase with distinct local crystalline order. This state is rather common for passive systems [36] but less obvious for active systems. At large aspect ratio and high density, stratified patterns emerge consisting of lanes driven in opposite directions. These structures are reminiscent of the laning patterns observed for mixtures of passive particles (i.e. with no internal driving force) driven in a macroscopic external field [37–40]. A similar phenomenon was unveiled recently in mixtures of active and passive rod-like particles [41]. For intermediate densities and aspect ratios, we find distinct chaotic states characterized by meso-scale turbulent flow patterns with a significant vorticity in the velocity field [42]. This type of active turbulence has been observed in microbial suspensions [8, 9, 42, 43]. Contrary to traditional turbulent flow observed at high-Reynolds-number passive fluids the vortices that make up the turbulent flow patterns have a uniform mesoscopic size irrespective of the density or particle shape.

In principle, the full variety of different emergent states advanced here should be verifiable for bacterial systems and artificial rod-like colloidal or granular micro-swimmers. In a recent study, the statistical properties of the turbulent states as predicted from the SPR model have been systematically compared with flow-field data of confined bacterial systems [44]. It would be interesting to pursue a more systematic comparison with bacterial systems and assemblies of man-made micro-swimmers in order to verify the full topology of the predicted phase diagram.

The remainder of this paper is organized as follows: in section 2 we specify our model for self-propelled rods, the corresponding equations of motion and the simulation methodology. Numerical results on the non-equilibrium phase diagram are presented and analysed in section 3. We conclude in section 4 with a brief discussion of possible extensions of the model and we highlight opportunities to observe the predicted behaviour in experiment.

2. Frictional dynamics of a self-propelled-rod (SPR) model

One of the simplest ways to envisage a suspension of active mesogens is by considering a collection of rigid, self-propelled rods each moving with a constant self-propulsion force F directed along the main rod axis (see figure 1). Mutual rod repulsion is implemented by discretizing each rod into n spherical segments and imposing a repulsive Yukawa force with characteristic decay length λ between the segments of any two rods, such that λ defines the effective diameter of the rod of length ℓ [31]. If two sufficiently long rods perform a pair-collision, the interaction results in an effective nematic (apolar) alignment while the centres-of-mass attain a certain minimal distance due to the repulsive Yukawa forces. The potential energy of a rod pair α and β with orientation unit vectors $\{\hat{\mathbf{u}}_\alpha, \hat{\mathbf{u}}_\beta\}$ and centre-of-mass distance $\Delta\mathbf{r}_{\alpha\beta}$, is given by

$$U_{\alpha\beta} = \frac{U_0}{n^2}\sum_{i=1}^{n}\sum_{j=1}^{n}\frac{\exp[-(r_{ij}^{\alpha\beta}/\lambda)]}{r_{ij}^{\alpha\beta}} \tag{1}$$

where U_0 is the potential amplitude, λ the screening length, and

$$r_{ij}^{\alpha\beta} = |\Delta\mathbf{r}_{\alpha\beta} + (l_i\hat{\mathbf{u}}_\alpha - l_j\hat{\mathbf{u}}_\beta)|, \tag{2}$$

the distance between the ith segment of rod α and the jth segment of rod β, with $l_i \in [-(\ell-\lambda)/2, (\ell-\lambda)/2]$ denoting the position of segment i along the symmetry axis of the rod α. The screening length λ defines the effective diameter of the segments such that we may introduce an aspect ratio $a = \ell/\lambda$ to quantify the effective anisometry of the SPR. The case $a = 1$ corresponds to a single Yukawa point particle ($n = 1$). For $a > 1$, the number of segments per rod is fixed as $n = 3$ for $1 < a \leq 3$ and $n = \lfloor 9a/8 \rceil$ for $a > 3$ with $\lfloor\cdot\rceil$ denoting the nearest integer.

We focus on the dynamical regime relevant to microorganisms and artificial self-motile colloidal mesogens and we assume the motion of the SPRs to be overdamped due to solvent friction (in the zero Reynolds number limit). Since we are interested in the collision-dominated dynamics

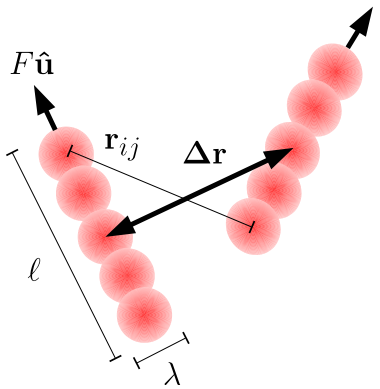

Figure 1. Coarse-grained representation of a pair of rod-like micro-swimmers with $n = 5$ repulsive Yukawa segments and aspect ratio $a = \ell/\lambda$. Self-propulsion is provided by a constant force F acting along the main rod axis indicated by the orientational unit vector $\hat{\mathbf{u}}$. The total rod pair potential is obtained by a sum over all Yukawa segment pairs with distance $\mathbf{r}_{ij}$ and is a function of the centre-of-mass distance vector $\Delta\mathbf{r}$ and orientations (equation (1)).

in dense suspensions, we disregard any thermal and intrinsic fluctuations in the swimming direction of the SPRs [4]. These fluctuation will be briefly discussed in section 3.4. Owing to their typical size of several microns, thermal fluctuations exerted by the solvent are deemed small for most bacterial and colloidal micro-swimmers which typically operate in the regime of large Péclet number where self-propulsion dominates Brownian motion [4, 42]. In the absence of noise the resulting equations of motion for the centre-of-mass $\mathbf{r}_\alpha(t)$ and orientation $\hat{\mathbf{u}}_\alpha(t)$ of each SPR are entirely deterministic and can be written compactly as

$$\mathbf{f}_{\mathrm{T}} \cdot \partial_t \mathbf{r}_\alpha = -\nabla_{\mathbf{r}_\alpha} U + F\hat{\mathbf{u}}_\alpha, \tag{3}$$

$$\mathbf{f}_{\mathrm{R}} \cdot \partial_t \hat{\mathbf{u}}_\alpha = -\nabla_{\hat{\mathbf{u}}_\alpha} U. \tag{4}$$

Here, F is a constant self-motility force acting along the longitudinal axis of each rod (figure 1), $U = (1/2)\sum_{\beta,\alpha:\beta\neq\alpha} U_{\alpha\beta}$ the total potential energy, $\nabla_{\hat{\mathbf{u}}}$ denotes the gradient on the unit circle, and

$$\mathbf{f}_{\mathrm{T}} = f_0\left[f_\parallel \hat{\mathbf{u}}_\alpha\hat{\mathbf{u}}_\alpha + f_\perp(\mathbf{I} - \hat{\mathbf{u}}_\alpha\hat{\mathbf{u}}_\alpha)\right], \tag{5}$$

$$\mathbf{f}_{\mathrm{R}} = f_0 f_{\mathrm{R}}\mathbf{I}, \tag{6}$$

are the translational and rotational friction tensors ($\mathbf{I}$ is the two-dimensional (2D) unit tensor) with a Stokesian friction coefficient f_0. The dimensionless geometric factors $\{f_\parallel, f_\perp, f_{\mathrm{R}}\}$ depend solely on the aspect ratio a, and we adopt the standard expressions for rod-like macromolecules, as given in [45]

$$\frac{2\pi}{f_\parallel} = \ln a - 0.207 + 0.980a^{-1} - 0.133a^{-2}, \tag{7}$$

$$\frac{4\pi}{f_\perp} = \ln a + 0.839 + 0.185a^{-1} + 0.233a^{-2}, \tag{8}$$

$$\frac{\pi a^2}{3f_{\mathrm{R}}} = \ln a - 0.662 + 0.917a^{-1} - 0.050a^{-2}. \tag{9}$$

It is expedient to multiply equation (3) with the inverse matrix $\mathbf{f}_{\mathrm{T}}^{-1}$:

$$\partial_t \mathbf{r}_\alpha = v_0\hat{\mathbf{u}}_\alpha - \mathbf{f}_{\mathrm{T}}^{-1} \cdot \nabla_{\mathbf{r}_\alpha} U, \tag{10}$$

where

$$v_0 = \frac{F}{f_0 f_\parallel}, \tag{11}$$

defines the self-propulsion velocity of a non-interacting SPR.

In our simulations, we have adopted characteristic units such that $\lambda = 1$, $F = 1$, and $f_0 = 1$, which means that distance is measured in units of λ, velocity in units of F/f_0, time in units of $\tau_0 = \lambda f_0/F$, and energy in units of $F\lambda$. Upon rescaling to dimensionless coordinates, three relevant system parameters remain: the dimensionless Yukawa amplitude $\tilde{U}_0 = U_0/(F\lambda)$, which determines the hardness of the rod interactions relative to their characteristic propulsion energy, the aspect ratio a, and the effective volume fraction of the system

$$\phi = \frac{N}{A}\left[\lambda(\ell - \lambda) + \frac{\pi\lambda^2}{4}\right], \tag{12}$$

where the term between brackets denotes the 2D volume A_{rod} of a spherocylindrical rod. For steeply repulsive Yukawa interactions, the general dynamical behaviour resembles that of hard rods and only weakly depends on the Yukawa amplitude, and we fix $\tilde{U}_0 = 250$. The remaining quantities, the rod shape a and volume fraction ϕ constitute the main steering parameters for our investigations. We simulate the evolution of the SPR coordinates as a function of time $\tau = t/\tau_0$ in a square box of length L with periodic boundary conditions at volume fractions in the range $0.05 < \phi < 0.9$. The simulations are carried out using a time discretization $\Delta\tau = 0.002\rho^{-1/2}$, where $\rho = N\lambda^2/A$ with typically $N = 10^4$ rods per simulation. Initial configurations, generated from a rectangular lattice of aligned rods with $\hat{\mathbf{u}}$ pointing randomly up or down are allowed to relax during an interval $\tau = 1000$ before statistics are gathered over an interval $\tau = 20L$ with $L = (N/\rho)^{1/2}$ the dimension of the simulation box (in units of λ). Velocity vector fields $\mathbf{v}(\mathbf{r}, t)$ are constructed by measuring the average centre-of-mass velocity within sub-cells centred around the position $\mathbf{r}$. To this end we project the particle positions onto a 2D cubic grid $\{(i, j) \mid 1 \leq i, j \leq G\}$ and measure the average velocity $\mathbf{v}(t; i, j)$ in each bin (i, j) at a given time t. In order to test for finite size effects, we consider two different system sizes: small systems with $N = 1 \times 10^4$ particles and large systems with $N = 4 \times 10^4$ particles at the same filling fraction ϕ. The coarse-graining parameter G is chosen adaptively such as to ensure that each bin represents the average velocity of about 10 SPRs. Generally, we observe that the dynamical structure and order parameters of the emergent states are robust with respect to changes in the particle number N, provided N is at least of $\mathcal{O}(10^4)$.

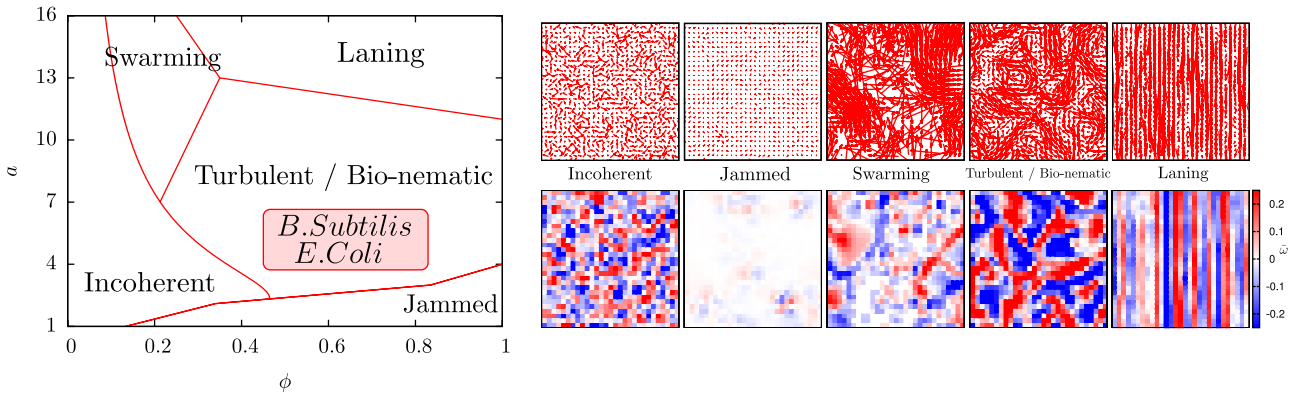

Figure 2. Schematic non-equilibrium phase diagram of the 2D SPR model at variable aspect ratio a and effective filling fraction ϕ. Values exceeding unity are, in principle, possible due to the softness of the Yukawa interactions. The area relevant to self-motile bacteria is highlighted in red. A number of distinctly different dynamical states are discernible as indicated by the coarse-grained maps of the velocity field $\mathbf{v}(\mathbf{r}, t)$ (upper panels) at time t and the corresponding scalar vorticity field $\tilde{\omega}(\mathbf{r}, t) = [\nabla \times \mathbf{v}(\mathbf{r}, t)] \cdot \hat{\mathbf{e}}_z$ (lower panels) expressed in units of τ_0^{-1}.

3. Results

3.1. Non-equilibrium phase diagram for the SPR model

Upon varying the effective volume filling fraction ϕ and the rod aspect ratio a a number of qualitatively different dynamical phases emerge. A schematic non-equilibrium phase diagram, shown in figure 2, illustrates the importance of the SPR anisometry in determining the stationary dynamical state of the system. The low-density regime is generally characterized by disordered motion with little or no dynamical coherence. Beyond a certain threshold density cooperative motion becomes manifest and translates into dynamical states whose structure depends on the intrinsic 'aligning force' of the SPRs. Short rods generally jam at high packing fractions whilst very long rods ($a > 13$) exhibit swarming behaviour with large spatio-temporal density fluctuations. The swarming and laning phases adjoin a large region of bio-nematic and turbulent flow characterized by vortices and extended nematic jet-like structures [42, 46].

Generally, the transitions from the dilute phase to regimes with strong cooperative motion can be localized by the 2D Onsager overlap density [47], defined as the density corresponding to a single rod occupying an average area equal to its excluded area $A_{\rm ex} = (2/\pi)(\ell-\lambda)^2+(\pi/4)\lambda^2$. The latter expression can be derived from the rod dimensions in figure 1 by assuming a pair of spherocylindrical rods with isotropic orientations. By combining terms one arrives at the following expression for the overlap density:

$$\phi^* = \frac{A_{\rm rod}}{A_{\rm ex}} = \frac{1+4(a-1)/\pi}{1+8(a-1)^2/\pi^2}. \qquad (13)$$

In figure 2 we have plotted ϕ^* to mark the crossover from incoherent to cooperative turbulent and swarming motion. The overlap density thus demarcates the region where many-body rod collisions (exceeding the pair level) become important and various non-trivial emergent states arise. In the sections below we shall present a more detailed overview of the dynamical states and the crossovers indicated in figure 2.

3.2. Short rods: active jamming

For small aspect ratios ($a < 3$) a distinct transition towards a jammed state is observed upon increasing density. This behaviour is hinted at by the average SPR velocity for which we may probe both parallel and transverse contributions via

$$v_\parallel = \frac{1}{N}\left\langle \sum_{\alpha=1}^{N} \hat{\mathbf{u}}_\alpha \hat{\mathbf{u}}_\alpha(t) \cdot \mathbf{v}_\alpha(t) \right\rangle,$$
$$v_\perp = \frac{1}{N}\left\langle \sum_{\alpha=1}^{N} \left(\mathbf{I} - \hat{\mathbf{u}}_\alpha \hat{\mathbf{u}}_\alpha(t)\right) \cdot \mathbf{v}_\alpha(t) \right\rangle, \qquad (14)$$

where the brackets $\langle \cdots \rangle$ denote a time average. The results are depicted in figure 3. In general, the average parallel velocity decreases monotonically with density as the particles get progressively hindered in their motion due to mutual rod collisions. For small a the parallel mobility drops rapidly for larger ϕ, indicating a severe slowing down of the collective dynamics. This behaviour is more clearly reflected in the mean-square displacement (figure 4) where a sharp drop in the mobility (over nearly two orders of magnitude) at $\phi = 0.84$ marks the onset of jamming. Throughout the density range the motion is observed to be sub-ballistic at long times with $\langle r^2 \rangle \sim \tau^{1.75\pm0.1}$. Despite the high packing fraction the SPRs do not become fully caged on the timescale investigated due to the presence of remnant collective motion as evident from the velocity field in figure 4. This behaviour is different from the active jamming recently studied in a model system of soft active spheres where a much sharper transition from fluid-type to arrested dynamics was observed [48]. The jamming point depends strongly on particle anisometry as indicated in figure 2 with a marked shift towards higher volume fractions upon increasing a. From a structural point of view the jamming transition is accompanied by a crossover towards orientationally and positionally ordered structures, as evident from the marked degree of local crystalline order at large filling fractions. The velocity maps reveal small pockets of locally enhanced particle mobility which bear

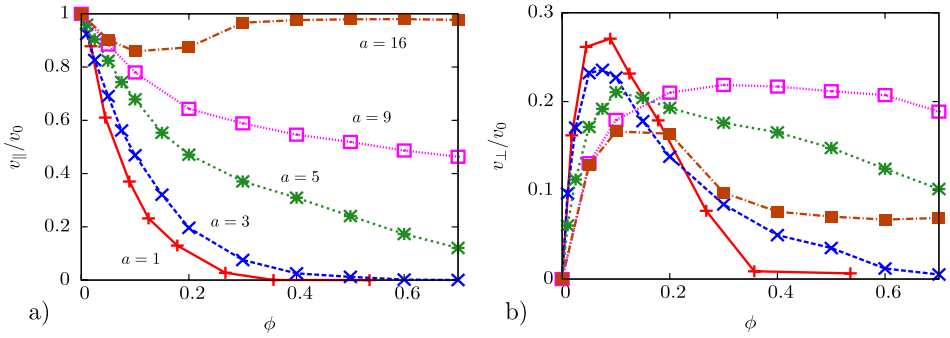

Figure 3. Evolution of the average SPR velocity as a function of filling fraction ϕ for a number of particle aspect ratios. The figure shows the average velocity component $v_\parallel$ along the main rod orientation (a) and the average perpendicular component $v_\perp$ (b), both expressed in units of the velocity v_0 of a free SPR.

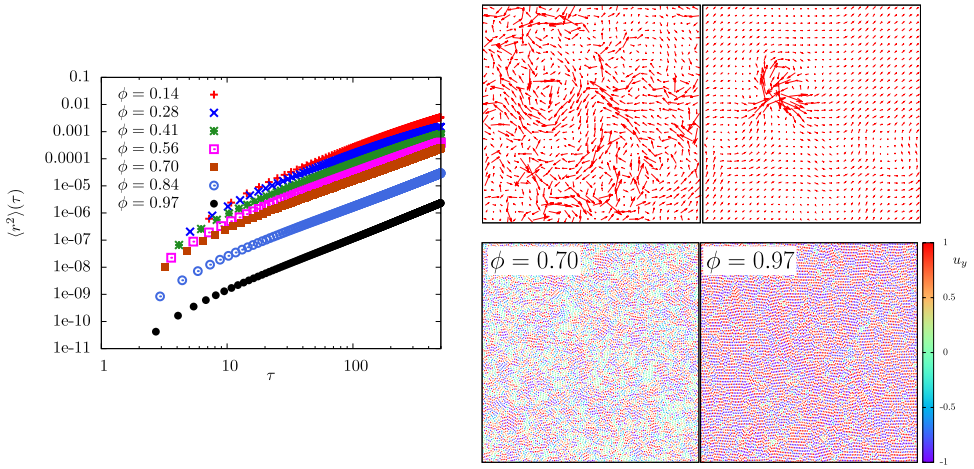

Figure 4. Mean-square displacement of the centre-of-mass for SPRs with aspect ratio $a = 3$. The snapshots depict velocity fields (upper panels) and the SPR coordinates (lower panels) for two different bulk filling fractions corresponding to a fluid state with turbulent signatures at $\phi = 0.70$ and a jammed state at $\phi = 0.97$. Colour coding is used to indicate the orientation $u_y = \hat{\mathbf{u}} \cdot \hat{\mathbf{e}}_\mathbf{y}$ of each rod.

some resemblance to dynamical heterogeneities commonly observed in glassy systems of passive thermalized colloids or granulates [49]. An intriguing avenue for future research could be to make a systematic comparison of the jamming and freezing transition for slightly anisometric SPRs with active and passive particle dynamics. A detailed account of freezing of self-motile spherical Yukawa particles has recently been reported in [50].

3.3. Intermediate aspect ratio: vortical states and turbulence

The maximum in the transverse SPR velocities depicted in figure 3(b) suggest that the SPRs exhibit some degree of collective swirling motion at moderate densities even at small aspect ratios. This type of motion becomes much more manifest at larger a where distinct vortical patterns arise akin to turbulent flow. The kinetic energy associated with local vortical motion can be measured from the enstrophy per unit area [51–53], which is defined as:

$$\Omega = \tfrac{1}{2}\langle|\overline{\tilde{\omega}(\mathbf{r},t)}|^2\rangle, \qquad (15)$$

where the overbar denotes a spatial average. For slender rods ($a \geq 3$) the mean enstrophy exhibits a pronounced maximum as a function of the volume fraction ϕ (figure 5(a)). This maximum signals the density at which vortical motion is maximal. In a bacterial suspension this extremum would correspond to the optimal concentration for fluid mixing. The range of aspect ratios over which turbulence flow is stable corresponds well with the typical aspect ratios of bacterial cell bodies, e.g. $a \sim 3$ for *Escherichia coli* and $a \sim 6$ for *Bacillus subtilis* (cf figure 2).

The typical size of the vortices that make up the turbulent flow patterns can be extracted from the equal-time velocity autocorrelation function (VACF) $g_v(r) = \langle \mathbf{v}(0,t) \cdot \mathbf{v}(\mathbf{r},t)\rangle$. This quantity can be obtained from the microscopic SPR coordinates $\{\mathbf{r}_\alpha, \mathbf{v}_\alpha\}$ via:

$$g_v(r) = \frac{\langle \sum_\alpha \sum_{\beta\neq\alpha} \delta(r - |\mathbf{r}_\alpha - \mathbf{r}_\beta|)(\mathbf{v}_\alpha \cdot \mathbf{v}_\beta - \langle v\rangle^2)\rangle}{\langle \sum_\alpha \sum_{\beta\neq\alpha} \delta(r - |\mathbf{r}_\alpha - \mathbf{r}_\beta|)(\langle v^2\rangle - \langle v\rangle^2)\rangle}. \qquad (16)$$

The decay of the VACFs in figure 5(b) reveals a typical vortex size of about $\sim 5\ell$, an estimate that seems rather insensitive to the bulk density and aspect ratio. Monotonically decreasing velocity correlations correspond to bio-nematic-type states where large-scale nematic jets and vortices coexist [42] whereas negative correlations (cf the curves for $a = 7$ and $\phi > 0.8$) represent more pronounced vortical motion reminiscent

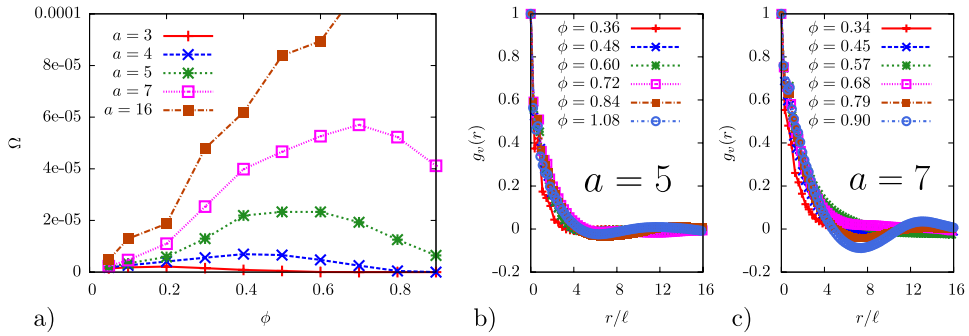

Figure 5. (a) Enstrophy Ω (in units τ_0^{-2}) versus filling fraction for a number of aspect ratios a in the turbulent regime. The maxima correspond to the densities where mixing due to vortical motion is the most efficient. (b) Spatial velocity autocorrelation function for a number of bulk volume fractions in the turbulent flow regime for two different aspect ratios a.

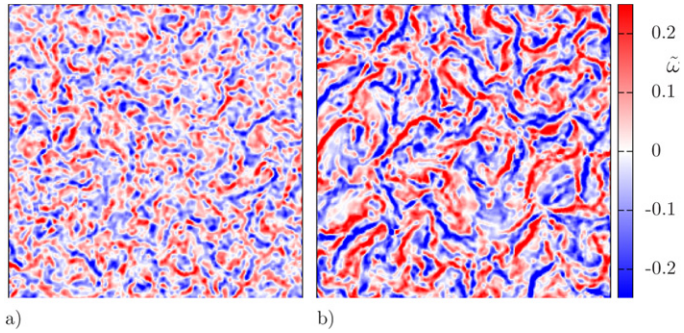

Figure 6. Maps of the vorticity field $\tilde{\omega}(\mathbf{r}, t) = [\nabla \times \mathbf{v}(\mathbf{r}, t)] \cdot \hat{\mathbf{e}}_z$ expressed in units of τ_0^{-1} showing large-scale turbulent flow for SPRs at intermediate aspect ratios: (a) $\phi = 0.72$, $a = 5$ and (b) $\phi = 0.90$, $a = 7$. The snapshots are based on $N = 4 \times 10^4$ SPRs. The lateral box dimensions are 103ℓ (a) and 78ℓ (b).

of fully developed meso-scale turbulent flow [44]. Typical vorticity snapshots are shown in figure 6.

In order to make a connection with classical 2D turbulence in high-Reynolds-number fluids we have calculated the energy spectrum which can be obtained as a Fourier transform of the VACF:

$$E(k) = \frac{k}{2\pi} \int \mathrm{d}\mathbf{r} \exp[-\mathrm{i}\mathbf{k} \cdot \mathbf{r}] \langle \mathbf{v}(0, t) \cdot \mathbf{v}(\mathbf{r}, t) \rangle. \qquad (17)$$

An alternative definition reads $\langle v^2 \rangle = 2 \int_0^\infty \mathrm{d}k\, E(k)$ where $E(k)$ reflects the accumulation of kinetic energy over different length scales. The results in figure 7 suggest asymptotic power-law scaling regimes for intermediate k-values with a power-law exponent close to the characteristic $k^{-5/3}$-decay predicted by the Kolmogorov–Kraichnan scaling theory [54, 55] for (passive) 2D turbulence in the inertial regime. In the present case, however, inertia is absent on the particle scale because the SPR motion is completely overdamped, but it is possible that the self-propulsion establishes 'effective' collective inertial effects on larger scales which could explain the observed $k^{-5/3}$ decay. Contrary to regular turbulent flow where energy is injected on the macroscopic scale, active turbulence is characterized by forcing on the microscopic scale. In general, the transport of kinetic energy towards smaller k becomes significantly damped on larger length scales [15] as highlighted by the low-k plateau in the power

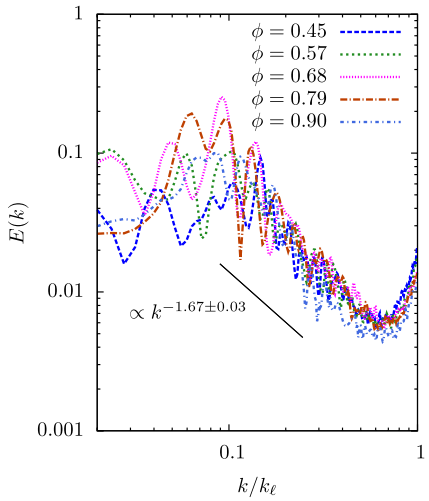

Figure 7. Power spectra of the kinetic energy for turbulent flow of SPRs with $a = 7$ ($k_\ell = 2\pi/\ell$). Universal scaling behaviour (with scaling exponent $-5/3$) is observed in the intermediate range of wavenumbers k.

spectra in figure 7. Indications for an upward enstrophy cascade with spectral scaling $E(k) \propto k^{-3}$ at length scales smaller then the injection scale have recently been reported from hydrodynamic theory of active fluids [56]. We refer

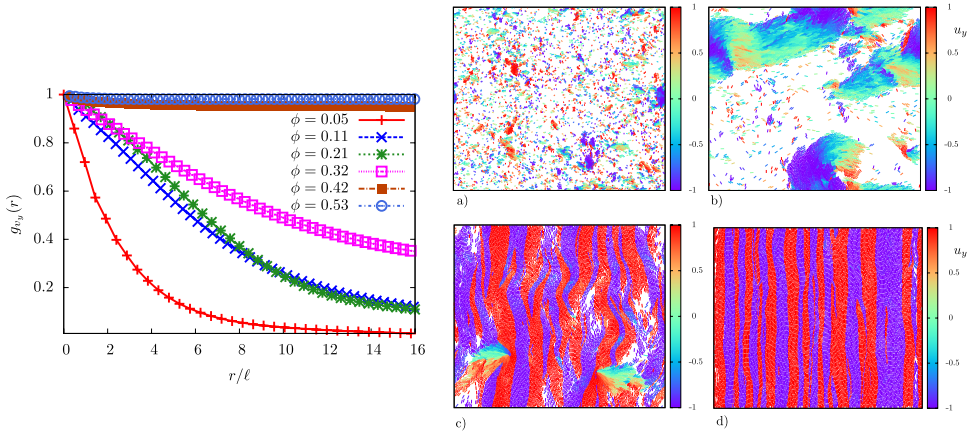

Figure 8. Spatial autocorrelation functions of the vertical velocity component $g_{v_y}(r)$ (equation (16)) at various filling fractions ϕ for SPRs with $a = 16$. Particle snapshots of the stationary states at (a) $\phi = 0.05$ (disordered, incoherent motion), (b) $\phi = 0.21$ (swarming), (c) $\phi = 0.32$ (initial stage of lane formation), and (d) $\phi = 0.42$ (fully developed laning state). The lateral box dimension corresponds to 38ℓ. Colour coding is used to indicate the orientation $u_y = \hat{\mathbf{u}} \cdot \hat{\mathbf{e}}_\mathbf{y}$ of each rod.

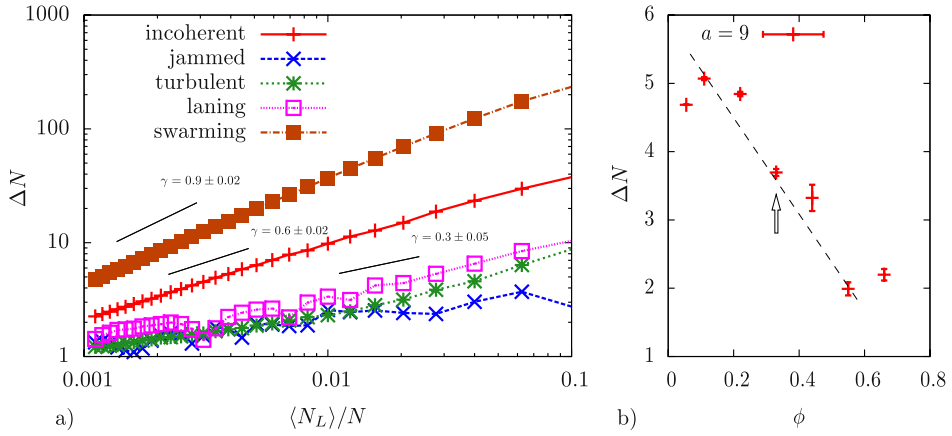

Figure 9. Number fluctuations $\Delta N^2 = \langle (N_L - \langle N_L \rangle)^2 \rangle$ as a function of the average particle number $\langle N_L \rangle$ (see text) in a system of $N = 1 \times 10^4$ SPRs. (a) Typical results for the different emergent states: the power-law scaling $\Delta N \propto \langle N_L \rangle^\gamma$ reveals giant number fluctuations ($\gamma \sim 1$) for the swarming case while fluctuations are strongly suppressed ($\gamma < 0.5$) in the dense states (jammed, turbulent and laning). (b) Density-dependence of the number fluctuations for SPRs with $a = 9$. The arrow locates the density where a crossover from swarming to turbulent flow can be expected upon increasing ϕ.

the reader to [44] for a more detailed discussion comparing meso-scale turbulence in active suspensions and regular high-Reynolds-number turbulent flow.

For small aspect ratios the vortical motion slowly dies out upon lowering the density in favour of incoherent, disordered motion. The crossover roughly takes place at the overlap density ϕ^* (equation (13)) which thus delimits the low-density boundary of turbulent flow. At larger aspect ratios the scenario is different. Here, density fluctuations become stronger and stronger upon lowering the density, and eventually cause the homogeneous vortical flow to break up into isolated polar swarms of SPRs separated by regions which are almost completely devoid of particles (see also figure 8(b)). In the high-density regime a sharp transition towards laning-type flow occurs due to a sudden 'stretching' of the vortices into stratified patterns. Both of these states will be described in more detail in the next section.

3.4. Long rods: swarming and lane formation

At low to moderate density, slender rods with $a > 10$ tend to form large compact flocks (figure 8(b)) which strongly resemble of the cooperative structures observed in large groups of organisms, e.g. schools of fish, flocks of birds [57, 58]. The dynamical swarming state is accompanied by anomalously large ('giant') number fluctuations as routinely found in active system [16–18, 30, 41, 59–61]. The results in figure 9(a) are obtained by measuring the fluctuation $\Delta N^2 = \langle (N_L - \langle N_L \rangle)^2 \rangle$ of the average number of SPRs $\langle N_L \rangle = NL^2/A$ present in a square sub-compartment of linear size L. From the power-law behaviour $\Delta N \propto \langle N_L \rangle^\gamma$ we can extract an exponent $\gamma = 0.9 \pm 0.2$ which is much larger than the value $\gamma = 0.5$ one would expect for a system in thermal equilibrium. The number fluctuations are much weaker for the incoherent state although the anomalous exponent ($\gamma \sim 0.6$) hints at some degree of clustering taking place even

at low densities [16] (cf figure 8(a)). For the dense states, fluctuations are strongly suppressed ($\gamma \sim 0.3$), which implies that the turbulent and laning flow can be regarded as nearly incompressible. The transition from swarming to turbulence at smaller aspect ratios can be located from a steep decrease in the density fluctuations at lower packing fractions as indicated in figure 9(b). The arrow thus locates a smooth crossover from strongly fluctuating flocking-type flow to homogeneous vortical flow where density fluctuations are strongly suppressed due to packing effects.

At larger volume fractions distinct laning patterns emerge that consist of cooperative stratified motion (figures 8(c)–(d)). The transition from flocking to laning as a function of the volume fraction can be localized from the equal-time VACF for the velocity components along the lane directions (in this case the vertical y-component). The characteristic decay of the VACF $g_{v_y}(r)$, shown in figure 8, allows a distinction between the disordered state at low densities where rod clusters are small and velocity correlations decay rapidly and the emergence of large cooperative flocks with velocity correlations spanning several dozens of rod lengths. A marked divergence of the correlation length occurs around $\phi \approx 0.4$ where the flocks start to span the entire system and self-organize into lanes moving in opposite directions. The same effect occurs if a is increased at fixed density and the crossover from turbulence to laning can be inferred from a sudden increase of the velocity correlation length. We remark that the preferred direction of the lanes along the y-axis is due to a small bias imparted by the squared simulation box and the periodic boundary conditions applied in both Cartesian directions. Similar laning patterns may appear along the horizontal axis if a different orientation of the rectangular lattice is used as a starting configuration. Other laning directions (e.g. along the diagonal) are favoured only transiently before collective redirection takes place along one of the easy axes of the simulation box. The considerable enstropy of the swarming state (figure 5) does not reflect homogeneous vortical flow but rather the curved trajectories of the isolated swarms which move with considerable speed owing to the strong local alignment and the low friction associated with slender rods (cf figure 3(a)). In the laning state the vorticity is strongly localized in the boundaries between adjacent layers moving in opposite directions. Here, the collective friction is even smaller than in the swarms and the average SPR velocity is close to the maximum swimming speed of a single SPR.

The laned flow patterns remain stable throughout the sampled time interval and no sign of break-up is observed over time even for large systems. We have verified the stability of the lanes against small fluctuations of the rod orientations that could be induced by thermal motion of the embedding medium or by some internal source, e.g. bacterial flagella. The rotational fluctuations are represented by a Gaussian white noise contribution $\Delta\hat{\mathbf{u}}$ to the equation of rotational motion of each rod α (cf equation (4)):

$$\partial_t \hat{\mathbf{u}}_\alpha = -\mathbf{f}_{\mathrm{R}}^{-1} \cdot \nabla_{\hat{\mathbf{u}}_\alpha} U + \Delta\hat{\mathbf{u}}_\alpha . \tag{18}$$

The stochastic term has zero mean $\langle \Delta\hat{u}_{i\alpha} \rangle = 0$ and correlations $\langle \Delta\hat{u}_{i\alpha}(t)\Delta\hat{u}_{j\beta}(t') \rangle = 2D_{\mathrm{R}}^{*}\delta_{ij}\delta_{\alpha\beta}\delta(t-t')$ (with $i = x, y$) in terms of some effective rotational diffusion rate D_{R}^{*}. Although 'run-and-tumble' motion as commonly observed in bacterial systems (notably *E. coli* [4]) is strictly non-Brownian at short times [62], its long-time behaviour is well captured by a rotational diffusion process with a diffusion constant much larger than the Stokes–Einstein value $D_{\mathrm{R}} = k_{\mathrm{B}}T/f_0 f_{\mathrm{R}}$ (where $k_{\mathrm{B}}T$ is the thermal energy) for passive Brownian rods. The strength of the tumbling motion is conveniently expressed in terms of the dimensionless tumbling parameter $\ell D_{\mathrm{R}}^{*}/v_0$, which is the ratio of the translation time a free SPR needs to swim over a distance ℓ and the typical tumbling time $1/D_{\mathrm{R}}^{*}$. Typical values for *E. coli* and other swimming bacteria are $\ell D_{\mathrm{R}}^{*}/v_0 \sim 0.01$ [4]. In the dense regime, the particle velocities are dominated by rod–rod collisions rather than thermal fluctuations and the intrinsic rotational diffusivity of the SPRs does not incur any qualitative change to the laning structures. In general, we assume that the spatio-temporal states and the topology of the phase diagram are robust against weak fluctuations in the swimming direction of the SPRs. We remark that similar laning states have been encountered in binary mixtures of SPRs with different self-motility at finite temperature [41]. In case of mixtures of active particles or macroscopically driven passive particles the laning instabilities can usually be rationalized from the disparity between the species mobility which favours segregated flow if the mobility ratio exceeds a certain threshold [37, 41]. In our case, however, such an intrinsic driving force is absent since all particles have equal microscopic mobility. We remark that banded and chaotic patterns of cooperative motion have been predicted recently in continuum descriptions of polar active particles [63–65] as well as in modified Vicsek models [33] which include nematic alignment [30] or density-dependent local mobility [66]. It would be intriguing to see if the laning patterns observed here can be reproduced from these models by means of a full account of the short-wavelength volume-exclusion correlations that are prevalent in dense systems of rigid SPRs.

4. Conclusions

We have studied the collective dynamical behaviour of a simple two-dimensional model of self-propelled rigid rods (SPRs) by means of numerical simulation. Depending on the rod shape and density, the SPR model exhibits a wealth of different emergent dynamical states including swarming, turbulence, laning and jamming. Although many of these states have been encountered in various setups, most notably (mixtures of) spherical particles in different external fields, the SPR model is able to generate these dynamical states upon variation of only two basic system parameters; the particle shape and density. The present approach may therefore serve as a benchmark to characterize the collective properties of different classes of self-motile organisms and artificial micro-swimmers of various shapes. As for the turbulent state, it was recently shown that the SPR model is capable of reproducing the velocity statistics obtained from experiments on strongly confined *B. subtilis* suspensions [44]. Future experiments on dense systems of self-propelled particles

with low and high particle anisometry will hopefully allow for similar comparisons for the jammed and laned state, respectively.

Future efforts could be aimed at extending the SPR model and the associated equations of motion by accounting for effects that could be relevant to concentrated bacterial systems. These include details of the self-propulsion mechanism and the associated many-body hydrodynamic interactions mediated by the solvent, particle flexibility and body forces transmitted by chemical gradients (chemotaxis) [42, 67]. The influence of stochastic forces could be incorporated if one wishes to assess the effect of translational and rotational noise (bacterial tumbling) in more detail. It is also desirable to explore the SPR model in three spatial dimensions, for instance, to study the phenomenology of fully developed three-dimensional meso-scale active turbulent flow which has been unexplored so far. Finally, it would be challenging to construct microscopic theories that are capable of linking the particle anisometry to the various emergent states observed in this study. Dynamical density functional theory for anisotropic particles [12, 32, 68, 69] could provide a promising avenue for this.

Acknowledgments

We are grateful to Jörn Dunkel, Julien Tailleur, Francesco Ginelli and Lyderic Bocquet for helpful discussions. Financial support from the DFG within SFB TR6 (project section D3) is gratefully acknowledged.

References

[1] Copeland M F and Weibel D B 2009 *Soft Matter* **5** 1174
[2] Koch D L and Subramanian G 2011 *Annu. Rev. Fluid Mech.* **43** 637
[3] Sokolov A and Aranson I S 2009 *Phys. Rev. Lett.* **103** 148101
[4] Drescher K, Dunkel J, Cisneros L H, Ganguly S and Goldstein R E 2011 *Proc. Natl Acad. Sci. USA* **108** 10940
[5] Kearns D B 2010 *Nat. Rev. Microbiol.* **8** 634
[6] Ramaswamy S 2010 *Annu. Rev. Condens. Matter Phys.* **1** 323
[7] Berg H C 2000 *Phys. Today* **53** 24
[8] Dombrowski C, Cisneros L, Chatkaew S, Goldstein R E and Kessler J O 2004 *Phys. Rev. Lett.* **93** 098103
[9] Sokolov A, Aranson I S, Kessler J O and Goldstein R E 2007 *Phys. Rev. Lett.* **98** 158102
[10] Riedel I H, Kruse K and Howard J 2005 *Science* **309** 300
[11] Saintillan D and Shelley M 2008 *Phys. Fluids* **20** 123304
[12] Baskaran A and Marchetti M C 2008 *Phys. Rev.* E **77** 011920
[13] Baskaran A and Marchetti M C 2008 *Phys. Rev. Lett.* **101** 268101
[14] Miño G, Mallouk T E, Darnige T, Hoyos M, Dauchet J, Dunstan J, Soto R, Wang Y, Rousselet A and Clement E 2011 *Phys. Rev. Lett.* **106** 048102
[15] Ishikawa T, Yoshida N, Ueno H, Wiedeman M, Imai Y and Yamaguchi T 2011 *Phys. Rev. Lett.* **107** 028102
[16] Volfson D, Kudrolli A and Tsimring L S 2004 *Phys. Rev.* E **70** 051312
[17] Narayan V, Ramaswamy S and Menon N 2007 *Science* **317** 105
[18] Deseigne J, Dauchot O and Chaté H 2011 *Phys. Rev. Lett.* **105** 098001
[19] Helbing D, Farkas I and Vicsek T 2000 *Nature* **407** 487
[20] Löwen H 2001 *J. Phys.: Condens. Matter* **13** R415
[21] Löwen H 2008 *J. Phys.: Condens. Matter* **20** 404201
[22] Erbe A, Zientara M, Baraban L, Kreidler C and Leiderer P 2008 *J. Phys.: Condens. Matter* **20** 404215
[23] Palacci J, Cottin-Bizonne C, Ybert C and Bocquet L 2010 *Phys. Rev. Lett.* **105** 088304
[24] Volpe G, Buttinoni I, Vogt D, Kummerer H J and Bechinger C 2011 *Soft Matter* **7** 8810
[25] Dreyfus R, Baudry J, Roper M L, Fermigier M, Stone H A and Bibette J 2005 *Nature* **437** 862
[26] Snezhko A, Belkin M, Aranson I S and Kwok W K 2009 *Phys. Rev. Lett.* **102** 118103
[27] Snezhko A and Aranson I S 2011 *Nature Mater.* **10** 698
[28] Peruani F, Deutsch A and Bär M 2006 *Phys. Rev.* E **74** 030904
[29] Peruani F, Starruß J, Jakovljevic V, Søgaard-Andersen L, Deutsch A and Bär M 2012 *Phys. Rev. Lett.* **108** 098102
[30] Ginelli F, Peruani F, Bär M and Chaté H 2010 *Phys. Rev. Lett.* **104** 184502
[31] Kirchhoff T, Löwen H and Klein R 1996 *Phys. Rev.* E **53** 5011
[32] Wensink H H and Löwen H 2008 *Phys. Rev.* E **78** 031409
[33] Vicsek T, Czirók A, Ben-Jacob E, Cohen I and Shochet O 1995 *Phys. Rev. Lett.* **75** 1226
[34] Kudrolli A, Lumay G, Volfson D and Tsimring L S 2008 *Phys. Rev. Lett.* **100** 058001
[35] Yang Y, Marceau V and Gompper G 2010 *Phys. Rev.* E **82** 031904
[36] Liu A J and Nagel S R 1998 *Nature* **396** 21
[37] Dzubiella J, Hoffmann G P and Löwen H 2002 *Phys. Rev.* E **65** 021402
[38] Rex M and Löwen H 2008 *Eur. Phys. J.* E **26** 143
[39] Wysocki A *et al* 2010 *Phys. Rev. Lett.* **105** 045001
[40] Vissers T, Wysocki A, Rex M, Löwen H, Royall C P, Imhof A and van Blaaderen A 2011 *Soft Matter* **7** 2352
[41] McCandlish S R, Baskaran A and Hagan M F 2012 *Soft Matter* **8** 2527
[42] Cisneros L H, Cortez R, Dombrowski C, Goldstein R E and Kessler J O 2007 *Exp. Fluids* **43** 737
[43] Wolgemuth C W 2008 *Biophys. J.* **95** 1564
[44] Wensink H H, Dunkel J, Heidenreich S, Drescher K, Goldstein R E, Löwen H and Yeomans J M 2012 Meso-scale turbulence in living fluids *Proc. Natl Acad. Sci. USA* at press
[45] Tirado M M, de la Torre J G and Martinez C L 1984 *J. Chem. Phys.* **81** 2047
[46] Cisneros L H, Kessler J O, Ganguly S and Goldstein R E 2011 *Phys. Rev.* E **83** 061907
[47] Onsager L 1949 *Ann. NY Acad. Sci.* **51** 627
[48] Henkes S, Fily Y and Marchetti M C 2011 *Phys. Rev.* E **84** 040301
[49] Berthier L, Biroli G, Bouchaud J P, Cipelletti L and van Saarloos W 2011 *Dynamical Heterogeneities in Glasses, Colloids and Granular Media* (Oxford: Oxford University Press)
[50] Bialké J, Speck T and Löwen H 2012 *Phys. Rev. Lett.* **108** 168301
[51] Danilov S D and Gurarie D 2000 *Usp. Fiz. Nauk* **170** 921
[52] Kellay H and Goldburg W I 2002 *Rep. Prog. Phys.* **65** 845
[53] Frisch U 2004 *Turbulence* (Cambridge: Cambridge University Press)
[54] Kraichnan R H 1967 *Phys. Fluids* **10** 1417
[55] Kraichnan R H and Montogomery D 1980 *Rep. Prog. Phys.* **43** 547
[56] Giomi L, Mahadevan L, Chakraborty B and Hagan M F 2012 *Nonlinearity* **25** 2245
[57] Toner J and Tu Y 1998 *Phys. Rev.* E **58** 4828
[58] Toner J, Tu Y and Ramaswamy S 2005 *Ann. Phys.* **318** 170
[59] Chaté H, Ginelli F and Montagne R 2006 *Phys. Rev. Lett.* **96** 180602

[60] Chaté H, Ginelli F, Grégoire G and Raynaud F 2008 *Phys. Rev.* E **77** 046113
[61] Zhang H P, Be'er A, Florin E L and Swinney H L 2010 *Proc. Natl Acad. Sci. USA* **107** 13626
[62] Tailleur J and Cates M E 2008 *Phys. Rev. Lett.* **100** 218103
[63] Mishra S, Baskaran A and Marchetti M C 2010 *Phys. Rev.* E **81** 061916
[64] Giomi L, Marchetti M C and Liverpool T B 2008 *Phys. Rev. Lett.* **101** 198101
[65] Giomi L, Mahadevan L, Chakraborty B and Hagan M F 2011 *Phys. Rev. Lett.* **106** 218101
[66] Farrell F D C, Tailleur J, Marenduzzo D and Marchetti M C 2012 *Phys. Rev. Lett.* **108** 248101
[67] Baskaran A and Marchetti M C 2009 *Proc. Natl Acad. Sci.* **106** 15567
[68] Rex M, Wensink H H and Löwen H 2007 *Phys. Rev.* E **76** 021403
[69] Wittkowski R and Löwen H 2011 *Mol. Phys.* **109** 2935